


Article

Cracking Pattern and Bearing Capacity of Steel Fiber-Reinforced Concrete Single-Layer Tunnel Lining

Huayun Li ¹, Yangfan Wu ^{1,*}, Anxiang Zhou ^{1,*}, Feng Lu ^{2,3}, Zhongcheng Lei ⁴, Bowen Zeng ⁵  and Kaicheng Zhu ¹¹ School of Architecture and Civil Engineering, Xihua University, Chengdu 610039, China² School of Emergency Management, Xihua University, Chengdu 610039, China³ Key Laboratory of Transportation Tunnel Engineering, Ministry of Education, School of Civil Engineering, Southwest Jiaotong University, Chengdu 610031, China⁴ Shenzhen Municipal Design & Research Institute Co., Ltd., Shenzhen 518029, China⁵ Department of Civil and Environmental Engineering, University of Alberta, Edmonton, AB T6G 2E9, Canada

* Correspondence: wuyangfan@stu.xhu.edu.cn (Y.W.); zhouanxiang@stu.xhu.edu.cn (A.Z.)

Abstract: In recent years, steel fiber-reinforced concrete (SFRC) single-layer linings have been used in tunnel engineering. Compared to plain concrete single-layer linings, SFRC single-layer linings demonstrate enhanced bearing capacity, durability, and sustainability. Existing studies primarily focused on the mechanical properties of SFRC; however, limited investigations have been conducted on the cracking pattern of SFRC linings. This study uses laboratory tests to examine the influence of steel fiber content and aspect ratio on the mechanical properties of concrete, such as compressive strength and elastic modulus. After the recommended content and aspect ratio of steel fiber are proposed through tests, the cracking pattern and safety performance of plain concrete and SFRC linings under surrounding rock pressure are studied using a similar model test. The test results indicate that the recommended steel fiber volume fraction and aspect ratio for CF35 SFRC are 0.58% and 70, respectively. Due to the effect of loose load, cracks initially develop on the inside of arch crowns in both plain concrete and SFRC single-layer linings. Subsequently, new cracks appear on the inside of the lining floor and the outside of the two wall feet. Numerous narrow cracks with rugged and winding expansion paths can be found on SFRC single-layer linings. Conversely, plain concrete single-layer linings exhibit fewer cracks with larger widths along a straighter path. The initial cracking load of a single-layer lining made of plain concrete is 0.027 MPa, whereas for a single-layer lining made of SFRC, it is 0.04 MPa. This indicates that SFRC can effectively enhance the initial cracking load of lining structures. In the event of damage to the lining, the most critical area for the plain concrete single-layer lining is at the two wall feet, where the minimum safety factor is 1.66. However, for the SFRC lining in the same location, the safety factor is 2.7, resulting in a 62.7% increase in safety.

Keywords: tunnel; single-layer lining; steel fiber-reinforced concrete; similar model test; cracking pattern



Citation: Li, H.; Wu, Y.; Zhou, A.; Lu, F.; Lei, Z.; Zeng, B.; Zhu, K. Cracking Pattern and Bearing Capacity of Steel Fiber-Reinforced Concrete Single-Layer Tunnel Lining. *Sustainability* **2023**, *15*, 10665. <https://doi.org/10.3390/su151310665>

Academic Editor: Ramadhansyah Putra Jaya

Received: 1 May 2023

Revised: 30 June 2023

Accepted: 4 July 2023

Published: 6 July 2023



Copyright: © 2023 by the authors. Licensee MDPI, Basel, Switzerland. This article is an open access article distributed under the terms and conditions of the Creative Commons Attribution (CC BY) license (<https://creativecommons.org/licenses/by/4.0/>).

1. Introduction

Steel fiber-reinforced concrete (SFRC) is a composite material that integrates short steel fibers into plain concrete in a random manner [1]. In recent years, SFRC has gained more and more popularity as a construction material [2,3] due to its superior mechanical properties, such as enhanced bearing capacity, durability, and cracking resistance. In tunnel construction, the single-layer lining was first proposed as a new support system in the 1970s. This lining system consists of single- or multi-layer concrete structures in which the primary support layer and the lining layer are integrated as a single entity, forming a support system capable of efficiently transferring stress between layers.

In tunnel construction, support linings composed of plain concrete structures are susceptible to excessive damage due to the brittleness of the material. For example, tunnel linings in high seismic intensity fault zones or weak surrounding rock regions are more

prone to cracking [4,5]. In contrast, as previously mentioned, SFRC tunnel lining structures exhibit superior mechanical properties [6–8]. The use of an SFRC lining enables the structure to maintain its deformation-resistant capability despite the presence of cracking, thereby enhancing overall structural performance. Additionally, the construction of SFRC single-layer linings is both convenient and cost-effective, rendering them an attractive option as a support structure in tunnel construction.

Extensive research has been conducted on the effect of steel fiber on concrete performance owing to the good performance of SFRC. It has been demonstrated that integrating steel fiber into concrete can improve compressive strength, the elastic modulus, and flexural strength [9–12]. Abbass et al. [13] investigated the effect of steel fibers with different lengths and diameters on the mechanical properties of concrete. The test results showed that the addition of steel fibers with varying content and lengths, along with increasing water-to-cement ratios, could increase compressive strength by approximately 10–25% and direct tensile strength by about 31–47%. Khabaz [14] proposed that when smooth and straight steel fibers are added to the concrete matrix, the bond between the fiber and the concrete is weak under tensile force. However, the bond strength between the fiber and concrete is enhanced when non-straight steel fibers are used. Zhang et al. [15] investigated the effect of three different steel fiber shapes on the mechanical properties of concrete through laboratory tests, discovering that the corrugated steel fiber had the most beneficial effect on compressive strength, splitting tensile strength, shear strength, and flexural strength. At the same time, the calculation formulas for compressive strength, splitting tensile strength, shear strength, and flexural strength were established and verified according to the test results. Al-Masoodi et al. [16] showed that steel fibers with rough surfaces can effectively enhance both the static and dynamic properties of concrete. Radojičić et al. [17] studied four kinds of straight steel fibers with different aspect ratios and two kinds of steel fibers with different shapes. The test results showed that as the steel fiber content increased, the workability decreased. However, with a continuous increase in steel fiber content, there is a continuous improvement in the mechanical properties and fracture properties of concrete. Liao et al. [18] indicated that, given the same fiber content, the optimal aspect ratio for SFRC to achieve the highest compressive strength was 50. In some harsh environments, steel fibers can also improve the durability of concrete. Niu et al. [19] suggested that an appropriate amount of steel fiber could delay the deterioration process of concrete under freeze–thaw cycles and reduce the propagation speed of concrete cracks. However, when the volume content of steel fiber exceeds 2%, it may have detrimental effects on the bond strength. Recent studies have shown that combining different fiber types can improve concrete performance in various aspects. Xu et al. [20] proposed that high fiber content in concrete may lead to ineffective fiber interweaving and that a mixture of 1.5 kg/m³ cellulose fiber and 1.0 kg/m³ polyvinyl alcohol fiber can better strengthen the mechanical strength of concrete. In addition to the mixed use of different types of steel fibers, SFRC showed better performance in terms of tensile strength and toughness than plain concrete when the ratio of steel fiber length to the maximum particle size of coarse aggregate ranged between 1.25 and 3; favorable compatibility between large particle size coarse aggregate and long steel fibers was also found [21,22]. Ige et al. [23] pointed out that SFRC with a maximum coarse aggregate size of 10 mm has better mechanical properties regardless of the type of steel fiber.

Steel fiber concrete has emerged as a competitive building material and is widely used in various engineering applications. In particular, fiber-reinforced concrete (FRC) when used in tunnel linings can enhance the structural performance of the tunnel and potentially replace conventional steel bars, thereby reducing the total cost of the project [24,25]. To enhance the construction efficiency and safety of tunnels, Johnson et al. [26] suggested that high-strength steel fibers in the range of 30–45 kg/m³; could serve as a reinforcement alternative to steel bars for single-layer tunnel linings. Caratelli et al. [27] discovered that incorporating 40 kg/m³ of steel fiber with an aspect ratio of 85 into precast concrete could improve cracking and fatigue resistance. Ding et al. [28] conducted experimental tests using

the symmetrical inclined beam method, and test results indicated that the combined use of steel fiber and stirrups enhances the bearing capacity and toughness of tunnel segment linings.

The majority of existing research focused on the influence of different lengths, aspects, and shapes of steel fibers on the mechanical properties of concrete (e.g., [9–18]), the appropriate content of steel fiber (e.g., [19]), and the ratio of steel fiber length and aggregate size (e.g., [21–23]). Meanwhile, studies on the application of SFRC in tunnel linings have mainly focused on the structural form and design method of SFRC single-layer linings (e.g., [24–26]), as well as the effect of SFRC on the bearing capacity and toughness of the lining (e.g., [27–33]). However, few studies have proposed that the mechanical properties of concrete can be improved best when the content of steel fiber and the ratio of length to diameter are different. Also, limited research has been performed on the cracking pattern of SFRC single-layer linings under surrounding rock pressure.

This paper initially investigates the effects of steel fiber content and aspect ratio on the mechanical properties of concrete through laboratory experiments. Based on the limited experimental program and the reference literature on SFRC, the recommended steel fiber content and aspect ratio are determined. Using the recommended steel fiber content and aspect ratio, a model test of an SFRC single-layer tunnel lining is conducted to study the tunnel's cracking pattern, crack distribution, and bearing capacity. This research can provide indications for the application of SFRC as a replacement for the plain shotcrete used in single-layer linings. It can also provide references for designing similar tunnel structures with single-layer linings, as well as for the maintenance and reinforcement of tunnel lining structures.

2. Experimental Analysis of the Mechanical Properties of SFRC

2.1. Test Materials and Mix Proportion

The concrete used in this study consisted of P·O42.5 cement, steel fiber, 3~15 mm continuous-graded gravel, ordinary river sand, water, a water-reducing agent, and grade I fly ash with a fineness modulus of 1.0, thus meeting the requirements of the Fly ash used for cement and concrete standard (GB/T 1596-2017) [34]. The steel fiber was a shear wave steel fiber with an equivalent diameter of 0.5 mm. The equivalent diameter was defined as that calculated when the steel fiber with a non-circular cross section was also regarded as an equivalent with a circular cross section. Type I steel fiber has a length of 25 mm and an aspect ratio of 50, while type II steel fiber has a length of 35 mm and an aspect ratio of 70. The steel fibers were produced by Jinjiang Road and Bridge Materials Co., Ltd., Hengshui City, Hebei Province, China. The steel fibers are shown in Figure 1. Ordinary river sand should have a fineness modulus greater than 2.5 and clay content of less than 3%. The water reducing agent was a carboxylic acid superplasticizer with a water reduction rate of 30% and a dosage of 0.8%. The addition of fly ash in concrete can effectively prevent alkali–aggregate reaction and enhance the durability of concrete. Tables 1 and 2 summarize the relevant information for the steel fiber and concrete, respectively.

Table 1. The performance parameters of steel fiber.

Steel Fiber Type	Length (mm)	Aspect Ratio	Equivalent Diameter (mm)	Density (g/cm ³)	Tensile Strength (MPa)	Elasticity Modulus (GPa)	Elongation at Break (%)
I	25	50	0.5	7.8	950	210	0.5–3.5
II	35	70					

Table 2. Mix proportion of C35 concrete.

Cement (kg)	Fly Ash (kg)	Sand (kg)	Graded Gravel (kg)	Water (kg)	Admixture (kg)
410	45	672	1100	190	8

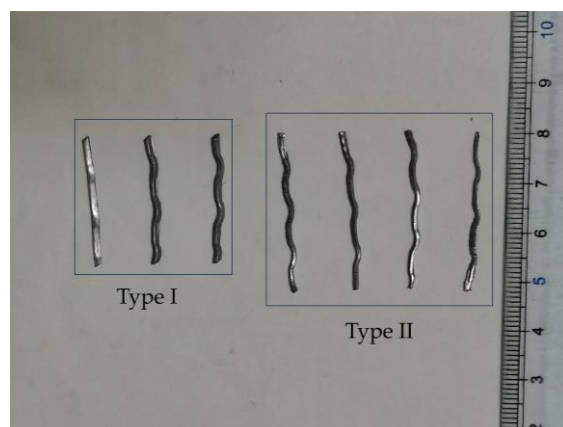


Figure 1. Steel fiber used in the experimental tests.

2.2. Specimen Preparation

The test specimens were prepared by following the parameters outlined in Standard test methods for fiber reinforced concrete (CECS 13: 2009) [35]. Several mechanical properties were obtained, including cubic compressive strength, axial compressive strength, and the elastic modulus. Details about the specimen size, steel fiber dosage, steel fiber type, and tested specimen amount are illustrated in Table 3.

Table 3. Test contents and specimen requirements.

Test Contents	Specimen Sizes (mm)	Steel Fiber Dosage (kg/m ³)	Steel Fiber Type	Specimen Amounts
Cubic compressive strength	150 × 150 × 150	0/30/40/45	I~II	3
Axial compressive strength	150 × 150 × 300	0/30/40/45	I~II	3
Elastic modulus	150 × 150 × 300	0/30/40/45	I~II	3

In accordance with the test scheme, the specimens were prepared by pouring the concrete mixture using a forced mixer to ensure the uniformity of the mixture after the incorporation of steel fibers. The feeding sequence of the mixture and the pouring specimens are shown in Figure 2.

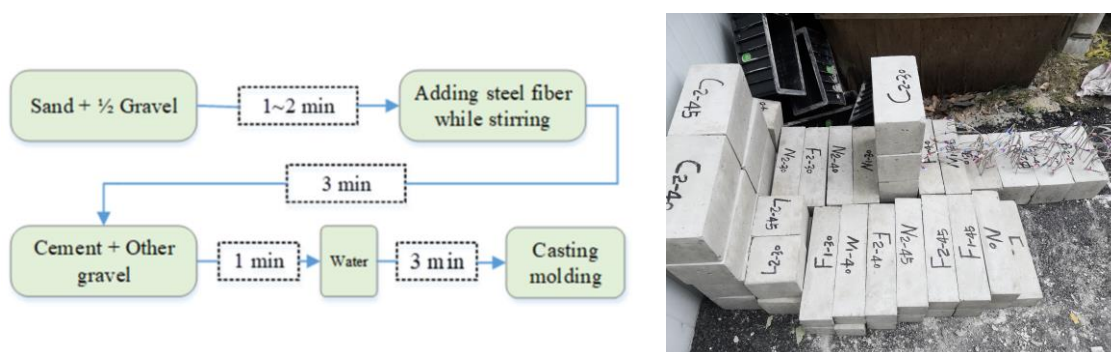


Figure 2. The feeding sequence and the molded specimens.

2.3. Compressive Strength Test Results

According to the Standard for test methods of concrete physical and mechanical properties (GB/T 50081-2019) [36], the compressive strength of SFRC was measured using a 2000 kN electro-hydraulic servo pressure testing machine with a loading rate of 0.5 MPa/s, as shown in Figures 3 and 4. The average compressive strength of each specimen is presented in Table 4.



Figure 3. Test of cubic compressive strength.



Figure 4. Test of axial compressive strength.

It can be seen from Table 4 that the compressive performance of concrete improves with the increase in steel fiber content. The improvement in the compressive strength of concrete for type I steel fiber is generally higher than that for type II steel fiber. The cubic compressive strength of L_{I-30} is 42.4 MPa, representing a 7.3% increase compared to L_0 . The cubic compressive strength of L_{I-40} is 44.0 MPa, representing a 11.4% increase compared to L_0 . The maximum cubic compressive strength of L_{I-45} is 44.9 MPa, representing a 13.7% increase compared to L_0 . In contrast, the cubic compressive strength of L_{II-45} is slightly less than that of L_{II-40} , with only a 7.3% relative increase compared to L_0 . This occurs due to the non-uniform distribution of steel fiber within the concrete matrix, resulting in an agglomeration effect. Axial compressive strength is positively correlated with the content of steel fiber. The maximum axial compressive strength of concrete with type I steel fiber and type II steel fiber is achieved at a dosage of 45 kg/m^3 .

When the steel fiber content was 30 kg/m^3 , the inclusion of type I and type II steel fibers increased axial compressive strength by 6.5% and 7.7%, respectively. When the steel fiber content was 40 kg/m^3 , the inclusion of type I and type II steel fibers increased axial compressive strength by 10.4% and 8.9%, respectively. When the steel fiber content was 45 kg/m^3 , the inclusion of type I and type II steel fibers increased axial compressive strength by 20.5% and 30.6%, respectively. However, due to the non-uniform distribution of steel fibers in the specimens, the size effect of the specimens, and the limited number of samples in this experiment, it is not possible to determine the precise enhancement pattern of steel fibers on the compressive strength of concrete. According to the study by Ezeldin et al. [37], it is known that the increase in compressive strength due to steel fibers should be

around 15%. Additionally, based on research by Nataraja et al. [38], it is known that with a constant aspect ratio of steel fibers, the compressive strength of concrete increases with increased steel fiber content within a certain dosage range. Therefore, it can be concluded that the maximum increase in the compressive strength of concrete is achieved with a steel fiber content of 45 kg/m³.

Table 4. SFRC compressive strength test statistics.

Steel Fiber Type	Steel Fiber Dosage (kg/m ³)	Specimen Number	Curing Time (d)	Average Failure Load (kN)	Average Compressive Strength (MPa)	
A. Cubic compressive strength						
Type I	30	L _{I-30}	30	954.0	42.4	
	40	L _{I-40}		990.0	44.0	
	45	L _{I-45}		1010.25	44.9	
Type II	30	L _{II-30}		918.0	40.8	
	40	L _{II-40}		960.75	42.7	
	45	L _{II-45}		954.0	42.4	
Plain concrete	0	L ₀		888.75	39.5	
B. Axial compressive strength						
Type I	30	C _{I-30}		30	618.75	27.5
	40	C _{I-40}	641.25		28.5	
	45	C _{I-45}	699.75		31.1	
Type II	30	C _{II-30}	625.5		27.8	
	40	C _{II-40}	632.25		28.1	
	45	C _{II-45}	758.25		33.7	
Plain concrete	0	C ₀	580.5		25.8	

Note: The specimen number subscript represents the corresponding steel fiber type and steel fiber content.

The reinforcement provided by steel fibers can work at both a micro and macro level. At a micro level, fibers arrest the development of microcracks, leading to higher compressive strengths, whereas at a macro level, fibers play a bridging role in concrete and control crack opening, thereby preventing the development of cracks and increasing the energy absorption capacity of the composite [39]. After the specimen is destroyed, due to the effect of steel fibers, the concrete still maintains a certain compressive strength. Steel fiber leads to concrete changing from brittle failure to ductile failure and improves the compressive properties of concrete.

2.4. Elastic Modulus Test Results

According to the Standard for test methods of concrete physical and mechanical properties (GB/T 50081-2019) [36], the initial load (F_0) is the one at which the stress is 0.5 MPa, and one in three of the axial compressive strengths of the specimen is determined as F_a for each test (calculated according to the corresponding value of axial compressive strength in Section 2.3). The specimen loading method is illustrated in Figure 5, and the test process is shown in Figure 6. The elastic modulus takes the secant modulus when the compressive stress is 1/3 of the axial compressive strength of the specimen. The elastic modulus test results of SFRC are summarized in Table 5.

Table 5 reveals that the B_{II-45} specimen had the maximum elastic modulus, which is 1.14 times the elastic modulus of B₀ and 1.06 times the elastic modulus of B_{I-45}. This is similar to the prediction of a 15% increase in elastic modulus proposed by Ezeldin et al. [37]. The increase rates of B_{I-30} and B_{I-40} in terms of the elastic modulus of concrete were 5.2% and 6.1%, respectively, while the increase rates of B_{II-30} and B_{II-40} in terms of the elastic modulus of concrete were 7.0% and 12.3%, respectively. Consequently, the increase rate for the elastic modulus of concrete for type II steel fiber is greater than that of type I steel fiber.

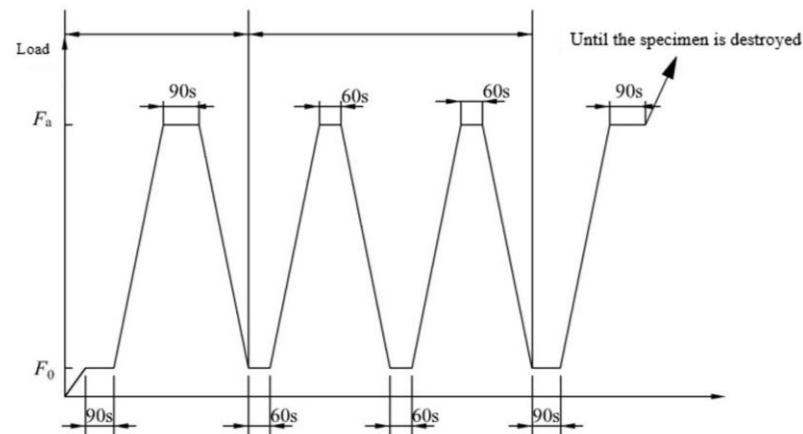


Figure 5. Loading process for the elastic modulus test.



Figure 6. Process for the elastic modulus test.

Table 5. SFRC elastic modulus test statistics.

Steel Fiber Type	Steel Fiber Dosage (kg/m ³)	Specimen Number	Curing Time (d)	Average Elastic Modulus (GPa)
Type I	30	B _{I-30}	30	34.3
	40	B _{I-40}		34.6
	45	B _{I-45}		35.2
Type II	30	B _{II-30}		34.9
	40	B _{II-40}		36.6
	45	B _{II-45}		37.2
Plain concrete	0	B ₀		32.6

Note: The specimen number subscript represents the corresponding steel fiber type and steel fiber content.

The length of type II steel fiber is greater than type I steel fiber, and in the 150 mm × 150 mm × 150 mm cube specimens, type I steel fiber showed better uniformity. Specimen distribution uniformity for type II steel fiber, however, was poor, resulting in a limited improvement in compressive strength, with type I steel fiber-reinforced concrete thus obtaining higher strength. The size of specimens used to test the elastic modulus was 150 mm × 150 mm × 300 mm, which is larger than the size of the specimens used to test cubic compressive strength, and the uniformity of the distribution of the two kinds of steel fibers in the specimen was better. Therefore, under the same uniformity condition, compared with the type I steel fiber, the type II steel fiber has a more significant effect on the mechanical properties of concrete. Longer fibers contribute to longer contact length,

resulting in improved force transfer and, consequently, an increased elastic modulus in concrete. Moreover, longer fibers create a larger bonding area within the concrete, which enhances interface bonding and improves the mechanical properties of the concrete. Therefore, it can be concluded that, with the same dosage, the steel fibers with a larger aspect ratio have a better effect on the improvement in elastic modulus. With the same aspect ratio, the elastic modulus also increases with the increase in steel fiber content [38].

The influence of different dosages of steel fibers on the mechanical properties of concrete varies. However, the dosage of 45 kg/m³ (volume fraction of 0.58%) generally leads to significant overall improvements in various aspects of concrete performance. There is certainly still room for improvement in the increase in steel fiber content, but the increase in steel fiber content has little effect on the mechanical properties of steel fiber-reinforced concrete. The 50 kg/m³ specimen was poured and stirred, and the steel fibers appeared to have undergone agglomeration and had poor fluidity [40]. Dă et al. [41] proposed that the phenomenon would eventually make it hard for the fibers to be completely filled in cement mortar as holes are formed when the steel fiber content is too great, which would first lead to stress concentration around the holes and then to cracks with the increase in stress. At the same time, based on the application of steel fiber-reinforced concrete in tunnel linings and due to the limitations of the spray mechanical properties used in the field, it is appropriate to determine a fiber content of 45 kg/m³. If the fiber content is increased, it easily blocks the pipe [42].

3. Study on the Cracking Pattern and Bearing Capacity of SFRC Single-Layer Linings

3.1. Design of a Similar Model Scheme

3.1.1. Information about the Prototype

The model test was conducted on a single-layer lining structure for a highway tunnel. The lining structure utilized CF35 SFRC with a thickness of 0.3 m, a span of 6.54 m, and a height of 7.07 m. The surrounding rock grade was classified as IV [43], and the tunnel was deeply buried [44].

3.1.2. Similarity Ratio of Tests

In conjunction with the lining prototype structure and test box dimensions, and considering the elimination of the boundary effect and the installation clearance requirements for monitoring components, the geometric similarity ratio of the model test was determined as 1:20 [45–48]. The tunnel lining was simulated using a gypsum mixture with an elastic modulus of 1~5 GPa. According to the values of elastic modulus obtained in Section 2.4 (34.3~37.2 GPa), the elastic modulus similarity ratio was 1:35. Using force, length, and time ([F]-[L]-[T]) as the basic dimensional system, the similarity coefficient of related physical quantities was derived according to the similarity criterion, as shown in Table 6.

Table 6. Similarity coefficients of the main physical quantities.

Physical Quantities	Physical Dimension	Similarity Relationship	Similarity Coefficient
Length l	L	S_l	20
Mass m	$FL^{-1}T^2$	$S_m = S_l^2 S_E$	14,000
Density ρ	$FL^{-4}T^2$	$S_\rho = \frac{S_E}{S_l^3}$	1.75
Stress σ	FL^{-2}	$S_\sigma = S_E$	35
Strain ε	-	$S_\varepsilon = 1$	1
Displacement x	L	$S_x = S_l$	20
Poisson ratio μ	-	$S_\mu = 1$	1
Elastic modulus E	FL^{-2}	S_E	35
Cohesion c	FL^{-2}	$S_c = S_E$	35
Internal friction angle φ	-	$S_\varphi = 1$	1
Force F	F	$S_F = S_l^2 S_E$	14,000

Given that the mechanical properties of similar materials for tunnel-surrounding rock and similar lining models meet the above similarity relationship, the thickness of the lining model was determined to be 1.5 cm, the width 32.7 cm, and the height 35.35 cm.

3.1.3. Similar Materials

(1) Similar materials of surrounding rock

According to the existing test conditions and referring to the successful research experience of scholars, five different proportions of mixtures were prepared with river sand, coarse quartz sand, fine quartz sand, fly ash, barite powder, and engine oil as the base materials, as shown in Table 7. The physical parameters of similar materials of surrounding rock with different mix ratios were proven by experiments, as shown in Table 8.

Table 7. Different mix proportions of the similar surrounding rock materials used in the tests.

Materials Ratio	Barite Powder	River Sand	Coarse Quartz Sand	Fine Quartz Sand	Engine Oil	Fly Ash
A	1	0.65	0.35	0.65	0.2	0.8
B	1	0.65	0.35	0.5	0.25	0.8
C	1	0.65	0.3	0.5	0.3	1.0
D	1	0.5	0.3	0.6	0.3	1.2
E	1	0.5	0.2	0.6	0.35	1.3

Table 8. Physical and mechanical parameters of the similar materials in surrounding rock for each group.

Groups	Parameters	Gravity/(kN/m ³)	Elastic Modulus/GPa	Cohesion/MPa	Internal Friction Angle/°	Poisson Ratio
	Prototype value	20~23	1.3~6	0.2~0.7	27~39	0.3~0.35
	Similar value	11.4~13.1	0.04~0.2	0.006~0.02	27~39	0.3~0.35
Test values	A	14.2	0.36	0.011	42.6	0.30
	B	13.2	0.22	0.010	41.1	0.32
	C	22.6	0.15	0.012	37.4	0.33
	D	12.9	0.25	0.017	35.2	0.30
	E	12.4	0.21	0.021	32.6	0.32

Through physical and mechanical property tests of the similar materials of surrounding rock with different mix ratios, slight adjustments to the mixture ratio, and further testing of the mixture until the mixture ratio was closest to the similarity requirements, it was determined that the similar materials of surrounding rock and the ratio were as follows: barite powder:river sand:coarse quartz sand:fine quartz sand:engine oil:fly ash = 1:0.56:0.39:0.72:0.33:1.33. The comparison between the physical and similar materials of surrounding rock and the physical and mechanical parameters of the class IV surrounding rock [43] is shown in Table 9.

Table 9. Physical and mechanical parameters of similar surrounding rock materials.

	Gravity (kN/m ³)	Elastic Modulus (GPa)	Cohesion (MPa)	Internal Friction Angle (°)	Poisson Ratio
Surrounding rock prototype value	22.5~24.5	1.3~6	0.2~0.7	27~39	0.3~0.35
Surrounding rock model value	13.14	0.19	0.018	36.7	0.31

(2) Similar materials for the lining structure

Based on the successful test experience of existing research [49,50], the steel fiber was simulated using experimental ultra-fine steel fiber to carry out the relevant model test, as shown in Figure 7. The content of steel fiber was determined according to the recommended content for steel fiber identified in the second chapter.



Figure 7. Extra-fine steel fiber for the tests.

In the mix design of similar materials for the SFRC single-layer lining model, a gypsum mixture was employed to simulate the desired properties. The steel fiber used in the test was wave-shaped, ultra-fine steel fiber. The primary considerations for the mix design of the lining model's similar materials were the compressive strength, elastic modulus, and Poisson ratio. Gypsum was the main material used in the lining model simulation, and the commonly used water–gypsum ratio ranged from 1.0 to 2.0. When the water–gypsum ratio was less than 1, it became challenging to control the material properties, while a water–gypsum ratio exceeding 2 resulted in easy segregation of the model mixture. To address these challenges, multiple sets of gypsum mixtures with varying water–paste ratios were designed, which incorporated barite powder and other additives, as shown in Table 10.

Table 10. Proportion design table of lining model materials.

		Group			
		Group 1	Group 2	Group 3	Group 4
Type	Type A	1:1.6:1.8:0.01	1:1.7:1.8:0.01	1:1.8:1.8:0.01	1:1.9:1.8:0.01
	Type B	1:1.6:1.5:1:0.01	1:1.7:1.5:1:0.01	1:1.8:1.5:1:0.01	1:1.9:1.5:1:0.01

Note: type A is gypsum:water:river sand:glue; type B is gypsum:water:barite powder:river sand:glue.

According to the mix ratio in Table 10, gypsum test blocks were poured. The size of the compressive strength test specimens was 100 mm × 100 mm × 100 mm, and three specimens in each group were fabricated according to different types and mix ratios. The size of the elastic modulus test specimen was 150 mm × 150 mm × 300 mm, and six specimens in each group were tested according to different types and different mix ratios. After the specimens were condensed and hardened, the specimens were placed in an indoor drying area. After the moisture on the surface of the specimen had dried, the specimen was placed in an oven for drying. When the quality of the test block was stable and unchanged, it could be determined that the test block had reached a dry state, and the relevant mechanical performance test could be carried out on the test block. The physical and mechanical properties of gypsum mixtures with different water–gypsum ratios were tested, as shown in Figure 8. The physical and mechanical parameters of gypsum specimens with different matching proportions were calculated, and the mean values of the test data are summarized in Table 11.

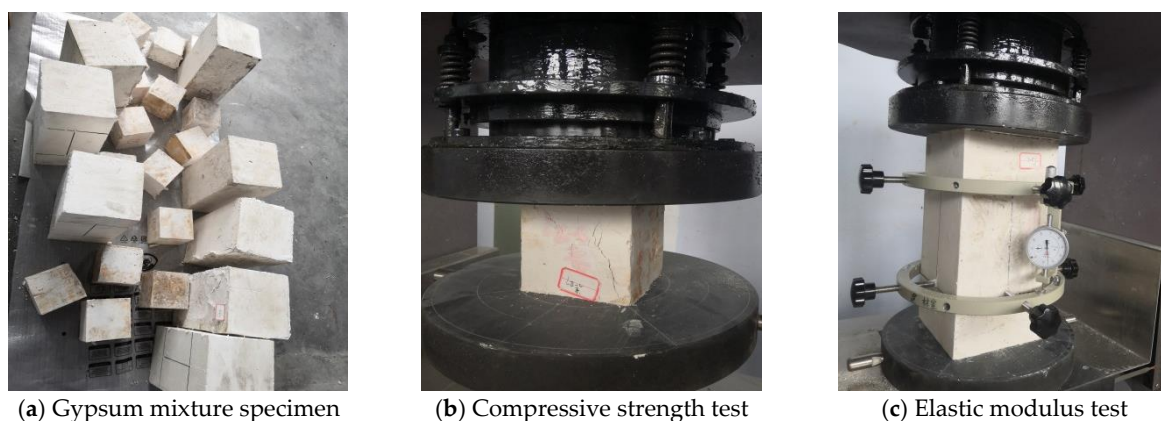


Figure 8. Mechanical property tests of gypsum specimens.

Table 11. Test data of gypsum specimens.

Parameters	Specimens							
	A-1	A-2	A-3	A-4	B-1	B-2	B-3	B-4
Compressive strength/MPa	1.53	1.34	1.27	1.13	1.42	1.23	1.17	1.04
Elastic modulus/GPa	1.257	1.184	1.026	0.873	1.136	1.054	0.866	0.731
Gravity/(kN/m ³)	9.24	8.36	8.21	7.64	11.67	11.22	10.89	10.33
Poisson ratio	0.21	0.22	0.21	0.22	0.20	0.21	0.23	0.22

Note: A-1 represents the experimental data of type A and group 1 in Table 10.

The physical and mechanical data of the B-2 specimen are closer to the theoretical values of the mechanical parameters of the lining model than the other groups, resulting in the composition and mix ratio of gypsum mixtures satisfying the similarity relationship (gypsum:water:barite powder:river sand:glue = 1:1.7:1.5:1:0.01). The comparison between the physical and mechanical properties of the lining prototype and lining modes is shown in Table 12.

Table 12. Comparison of the lining prototype and model's material mechanical parameters.

	Gravity (kN/m ³)	Elastic Modulus (GPa)	Cubic Compressive Strength (MPa)	Poisson Ratio
Lining prototype value	23.4	37.2	42.4	0.2
Lining model value	11.22	1.054	1.23	0.22

3.1.4. Test Preparation and Measuring Point Arrangement

According to the above similar material mix ratio for the lining, the steel fiber gypsum lining model was poured, and the plain concrete lining gypsum model was set as the control group. Strain gauges were pasted at the main position of the lining to monitor its mechanical changes. The lining model was prepared as shown in Figure 9. The model test platform is shown in Figure 10.

A micro earth pressure gauge was arranged on the outer surface of the lining to monitor the contact pressure between the lining structure and the surrounding rock, and the monitoring position is shown in Figure 11. Considering the lining clearance condition and structural symmetry, LVDT displacement meters were arranged at the four positions shown in Figure 12 to record displacement changes in the lining, and a high-definition numerical camera was used to capture crack generation and expansion of the lining structure during the test.

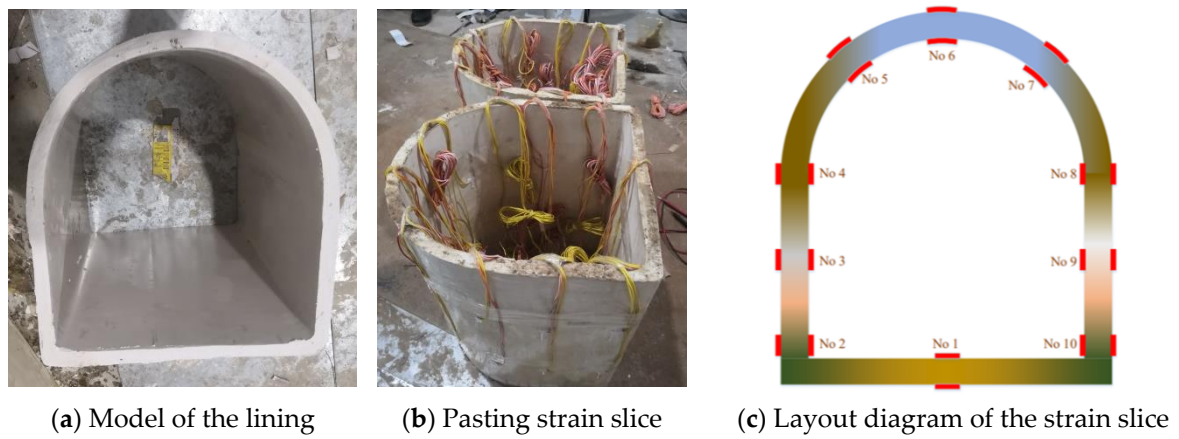


Figure 9. Preparation of the lining model.

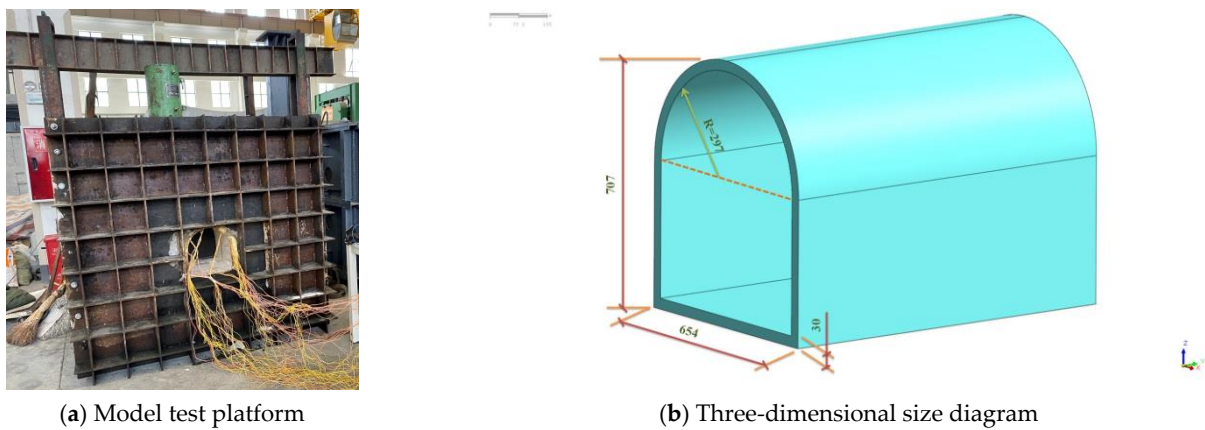


Figure 10. Test platform of the similar test model.

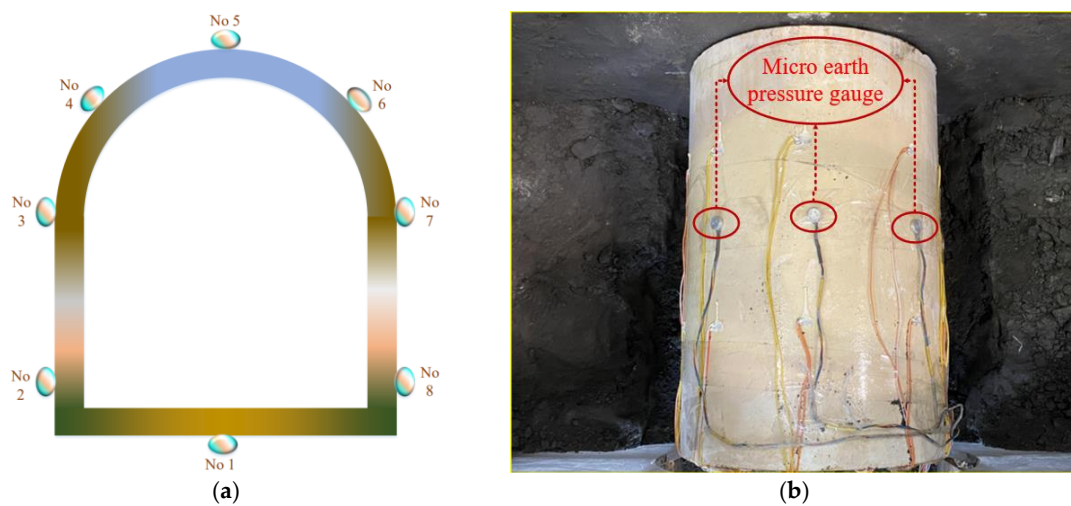


Figure 11. Layout of the micro earth pressure gauges. (a) Measuring point arrangement for the earth pressure gauge, (b) Micro earth pressure gauge.

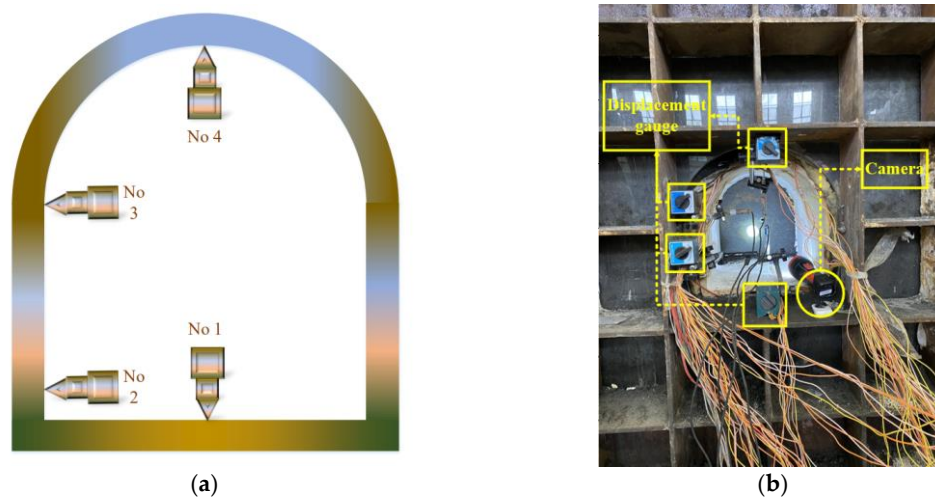


Figure 12. Layout of the displacement gauge and camera. (a) Displacement gauge measuring point layout, (b) Displacement gauge and camera.

3.1.5. Test Process

The configured materials similar to surrounding rock were laid into the model box, with each layer not exceeding 20 cm. The number of compactions was controlled to ensure that the physical and mechanical properties of the materials similar to surrounding rock met the requirements of the design. Upon reaching the design height, the lining model was placed on the filler, the micro earth pressure gauge (No. 1) was installed at the lining floor, and the layered filling was continued. In the process of layered filling, the micro earth pressure gauge was buried at the wall foot (No. 2, No. 8), side wall (No. 3, No. 7), arch shoulder (No. 4, No. 6), and arch crown (No. 5) of the lining, and it was ensured that the micro earth pressure gauge was in close contact with the lining surface. After all the monitoring components were arranged, the model was loaded according to the loading method in Table 13, where level 1 means a load of 9.81 kN is applied to the model (equivalent to 0.013 MPa) and the prototype load is equivalent to 0.467 MPa. Other levels have the same meaning.

Table 13. Step loading scheme for the model test.

Level	Model Load		Prototype Load (MPa)	Level	Model Load		Prototype Load (MPa)
	kN	MPa			kN	MPa	
Level 1	9.81	0.013	0.467	Level 5	49.03	0.067	2.333
Level 2	19.61	0.027	0.933	Level 6	58.84	0.080	2.800
Level 3	29.42	0.040	1.400	Level 7	68.65	0.093	3.267
Level 4	39.23	0.053	1.867	Level 8	78.45	0.107	3.733

3.2. Test Results and Analysis

3.2.1. Cracking Pattern of the Lining

Figure 13 displays the initial cracks observed in both the SFRC single-layer lining and the plain concrete single-layer lining during the test. The arch crown is located on the symmetric axis of the structure and is in the most unfavorable position, primarily subjected to vertical forces. Under the influence of a loose load, the initial cracks in both cases occur near the arch crown. Specifically, the linings in both cases exhibit the development of an initial primary crack on the inner side of the arch crown. As the load increases and the first crack emerges in the arch crown, subsequent cracks progressively appear near the lining floor and the two wall feet.

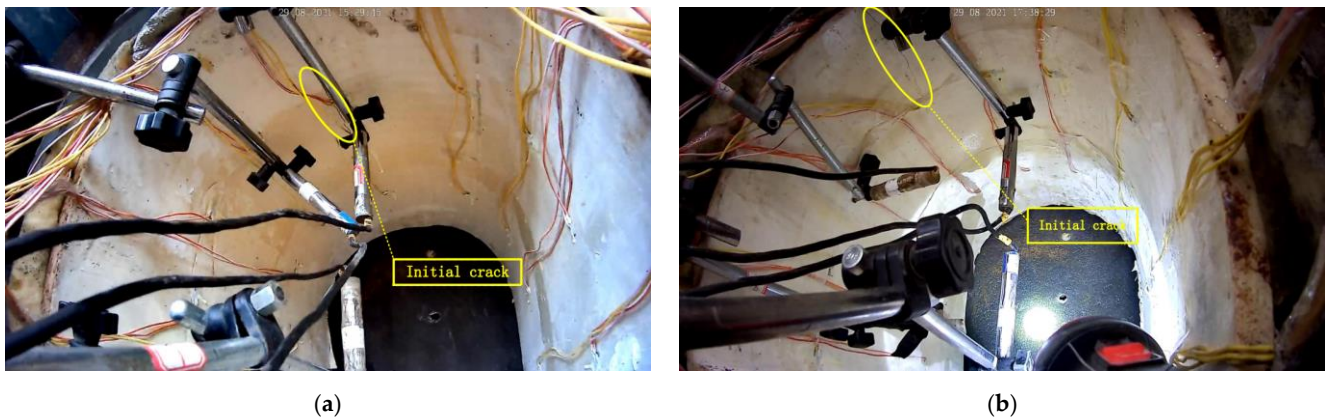


Figure 13. The initial crack location of the single-layer lining models. (a) The initial crack location of the SFRC single-layer lining model, (b) The initial crack location of the plain concrete single-layer lining model.

As the load increases, the cracks in the arch crown and lining floor progressively penetrate, with other parts gradually developing and expanding cracks. At a 58.84 kN load, the longitudinal crack in the SFRC single-layer lining arch crown reached 40% of the lining length and had a crack width of about 1.5 mm, as shown in Figure 14a. Meanwhile, the longitudinal cracks in the lining floor of the plain concrete single-layer lining structure had expanded to up to 70% of the lining length, and the cracks in the arch crown had reached 60%. The width and depth of the cracks were significantly larger than those in the SFRC single-layer lining. During the test, the crack opening amount at the lining floor was greater for both lining structures compared to other parts, with the cracking width gradually decreasing along the crack depth direction. At a load of 78.45 kN, the longitudinal cracks at the arch crown and lining floor of the plain concrete single-layer lining were almost entirely connected. A significant amount of small cracks were concentrated around the arch shoulder and wall foot regions. At this point, the lining structure lost its bearing capacity. Conversely, the longitudinal cracks in the arch crown of the SFRC single-layer lining model had basically penetrated 80% of the crown, retaining some bearing capacity.

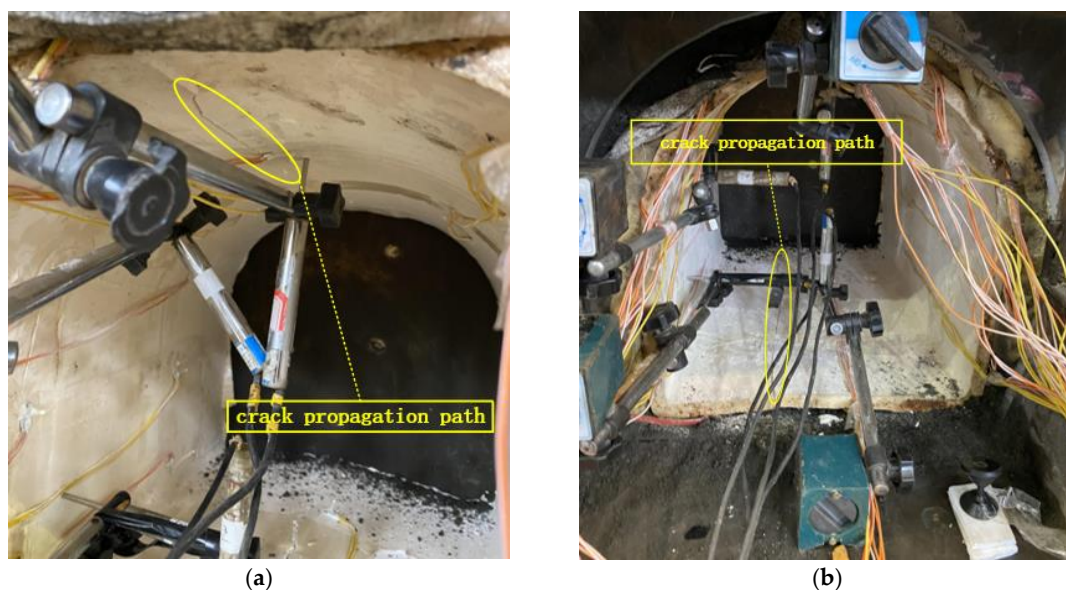


Figure 14. Crack propagation of single-layer linings. (a) Crack propagation path on the arch crown of the SFRC single-layer lining model, (b) Crack propagation path on the floor of the plain concrete single-layer lining model.

Figure 15 illustrates crack distribution in the lining model after failure. In the plain concrete lining structure, the first crack was initiated on the inner side of the arch crown. As the load increased, the crack rapidly widened and deepened. Eventually, the initial crack at the arch crown propagated throughout the entire structure, leading to complete destruction of the lining structure. At this point, the number of cracks in the plain concrete lining structure reached eight. On the other hand, in the SFRC lining structure, a very small longitudinal crack initially appeared at the arch crown. With the increasing load, the presence of steel fibers inhibited crack propagation, resulting in a gradual increase in crack depth. The path of crack development became tortuous, which delayed damage to the lining structure. While cracks did appear in other areas, no through cracks had formed yet. Ultimately, the tunnel lining exhibited a total of 14 cracks, demonstrating the beneficial effects of steel fibers in enhancing structural uniformity. The SFRC single-layer lining exhibited many narrow cracks with irregular and meandering expansion paths, while the plain concrete single-layer lining had wider cracks with simple and straight expansion paths. The wider and deeper cracks in the plain concrete single-layer lining were caused by the gradual increase in load, leading to a loss of tensile stress-bearing capacity in the lining matrix material at the cracks. This allowed main cracks in key parts to rapidly expand until they penetrated the entire lining structure, causing a loss of stability and bearing capacity. Due to the presence of cracks, the lining arch crown experienced uneven stress distribution, leading to stress concentration and causing the plain concrete lining arch crown cracks to deviate to the right. In contrast, the SFRC single-layer lining model experienced crack bridging due to the presence of steel fiber.

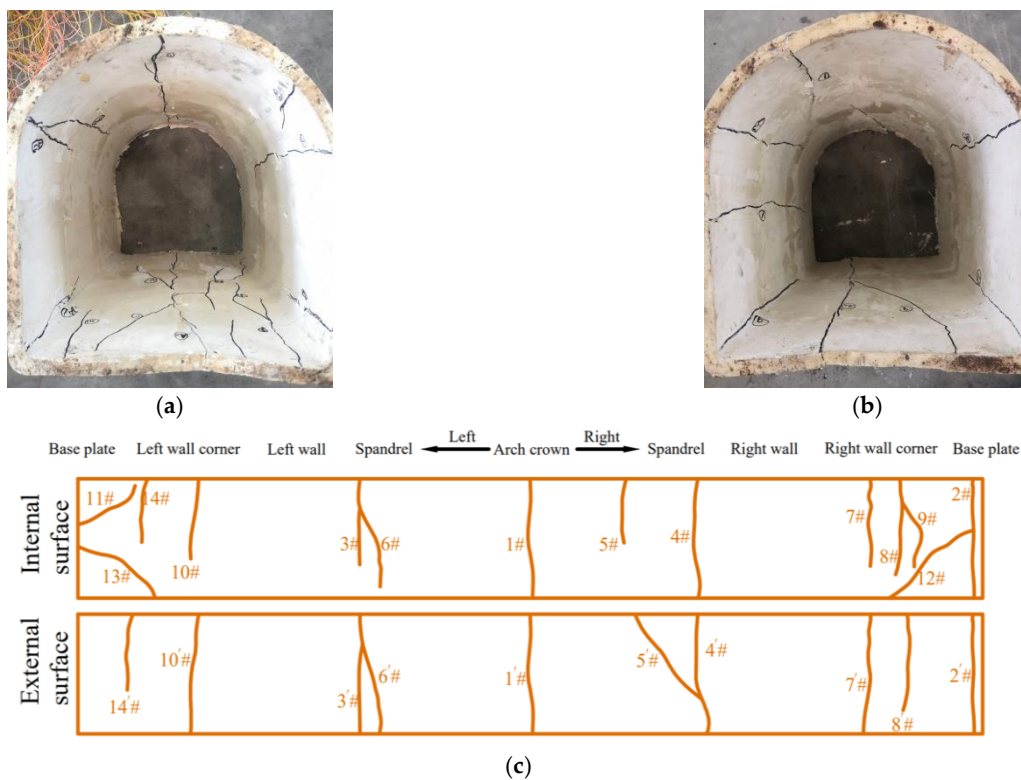


Figure 15. Cont.

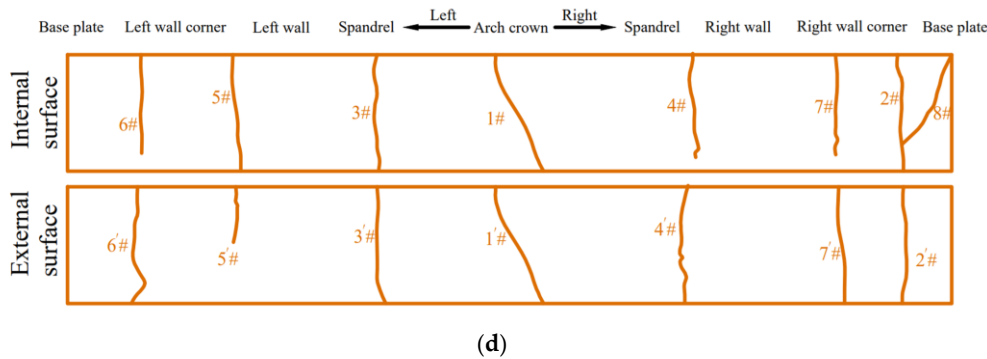
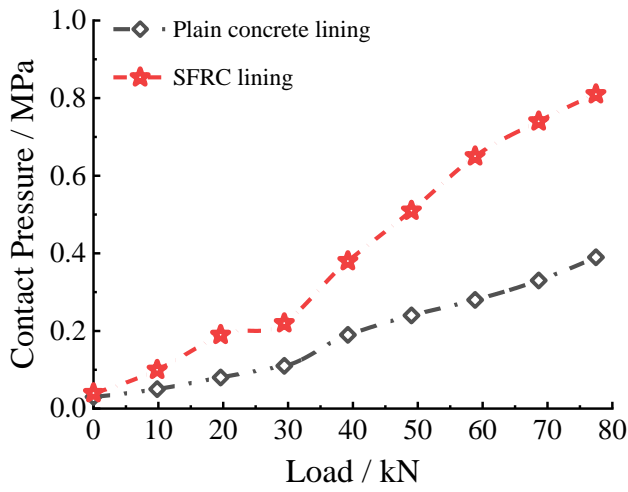


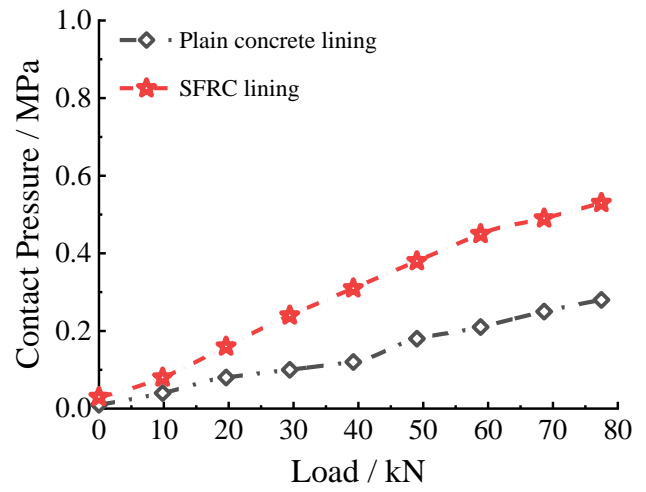
Figure 15. Distribution of single-layer lining cracks. (a) The overall distribution of cracks in the SFRC single-layer lining model, (b) The overall distribution of cracks in the plain concrete single-layer lining model, (c) Crack distribution diagram of the SFRC single-layer lining model, (d) Crack distribution diagram of the plain concrete single-layer lining model.

3.2.2. Contact Pressure between Linings and Surrounding Rock

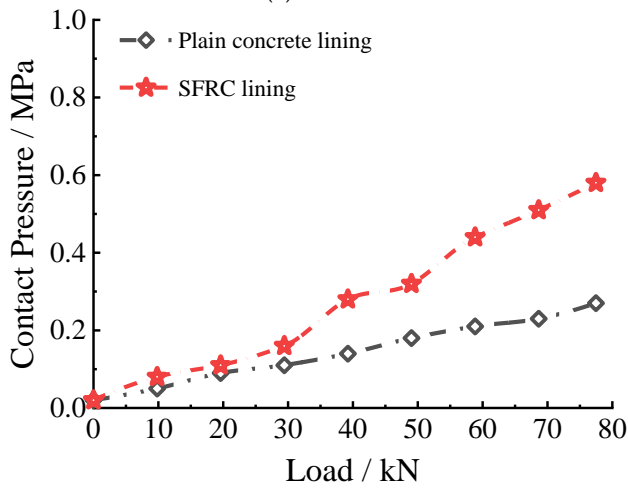
The relationship between the contact pressure between the lining and surrounding rock and the applied load is shown in Figure 16. It can be seen from Figure 16 that the contact pressure is positively correlated with the applied load, and the contact pressure between the SFRC single-layer lining and the surrounding rock is generally higher than that of the plain concrete single-layer lining. Figure 16a,e reveal that when the load increases to 29.42 kN, the contact pressure curve of the SFRC single-layer lining has a significant transition, indicating that the lining structure develops initial cracks at this time. When the load increased to twice the initial crack load, the lining structure still did not appear to be fully penetrated by longitudinal cracks. In contrast, the growth rate of the contact pressure curve of the plain concrete single-layer lining decreased at a load of 19.61 kN, and the contact pressure increased with increased load. When the load reached 63.74 kN, the arch crown and lining floor were rapidly squeezed into the tunnel, resulting in non-uniform structural deformation and stress distribution that caused a sharp increase in contact pressure (point 4 in Figure 16d). The underlying cause of this phenomenon is the formation of cracks in the lining as the load on the lining reaches a certain threshold. Consequently, the load is entirely borne by the internal steel fibers. As the load further increases, some steel fibers approach their yield or ultimate pullout strength, resulting in an increase in contact pressure. However, as the load continues to rise, the steel fibers yield or become dislodged, weakening the lining structure's resistance. This causes an increase in displacement at the corresponding section and unloads the contact pressure between the lining and the surrounding rock, ultimately leading to a sharp initial increase followed by a subsequent decrease in the contact pressure of the lining. When the load reached 78.45 kN, the contact pressures of the SFRC single-layer lining floor and arch crown were 0.82 MPa and 0.78 MPa, respectively, while other parts exhibited relatively low contact pressures.



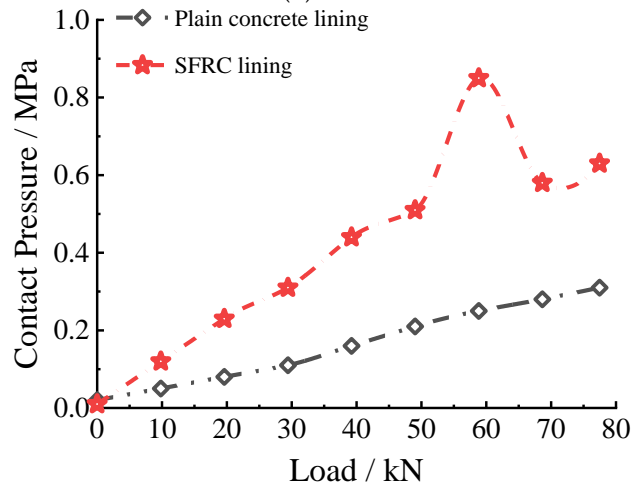
(a) Point 1



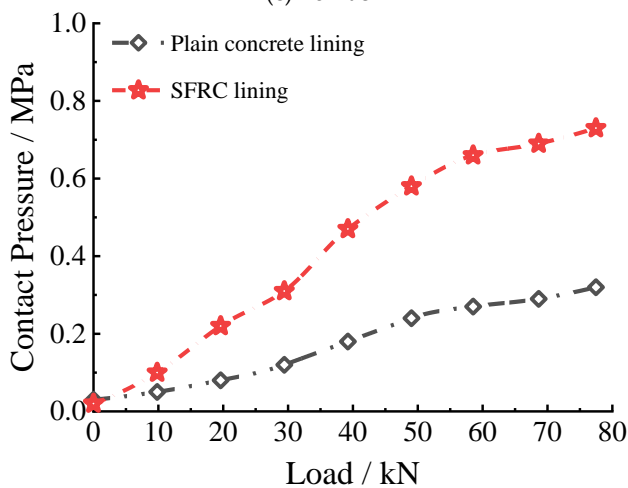
(b) Point 2



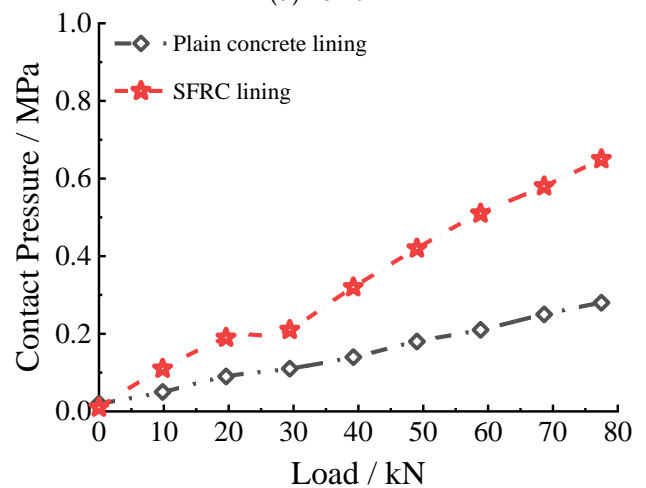
(c) Point 3



(d) Point 4



(e) Point 5



(f) Point 6

Figure 16. Cont.

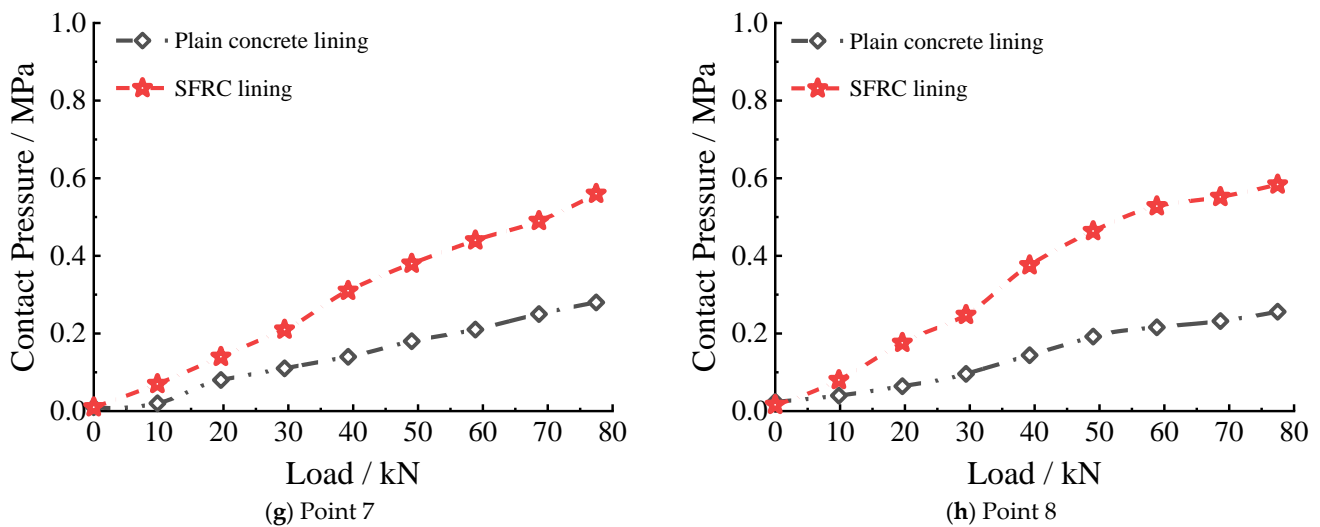


Figure 16. Contact pressure–load curves of single-layer lining models.

3.2.3. Radial Displacement

The load–displacement curves for each monitoring point are presented as shown in Figure 17, where the positive direction is defined as pointing towards the clearance direction of the lining structure. It can be seen from Figure 17 that the displacement of the two lining structures in each part increases with the increase in load, and the displacement of the arch crown, spandrel, and floor of the lining structure is positive during the loading process. Conversely, the displacement of the wall foot is negative, indicating that both lining structures undergo extrusion deformation at this location. The SFRC single-layer lining showed smaller displacement than that of the plain concrete single-layer lining. Additionally, the maximum displacement value of the two lining structures appeared at the arch crown of the plain concrete single-layer lining (reaching 13.2 mm), while the displacement of the SFRC single-layer lining at this position was 10.8 mm, which is an 18.2% reduction. During the loading process of the two lining structures, the soil beneath the lining bottom plate tended to be compacted, and the whole lining model produced downward displacement while the arch crown converged and deformed to the inner diameter of the hole under the action of the surrounding rock's load; thus, the displacement measured at the No. 4 monitoring point was large. From Figure 17a,d, it can be found that the load–displacement curves of the plain concrete single-layer lining turn when the pressure is 19.61 kN, and the slope of the curve increases there, indicating that the displacement of the plain concrete single-layer lining changes abruptly. It is shown that cracks occur in the plain concrete single-layer lining when the load is 19.61 kN. Conversely, the load–displacement curve of the single-layer SFRC lining increases sharply when the load is about 29.42 kN, indicating that there are cracks in the single-layer SFRC lining. The different cracking load indicates that the mechanical properties and cracking resistance of the SFRC lining are better than those of the plain concrete lining.

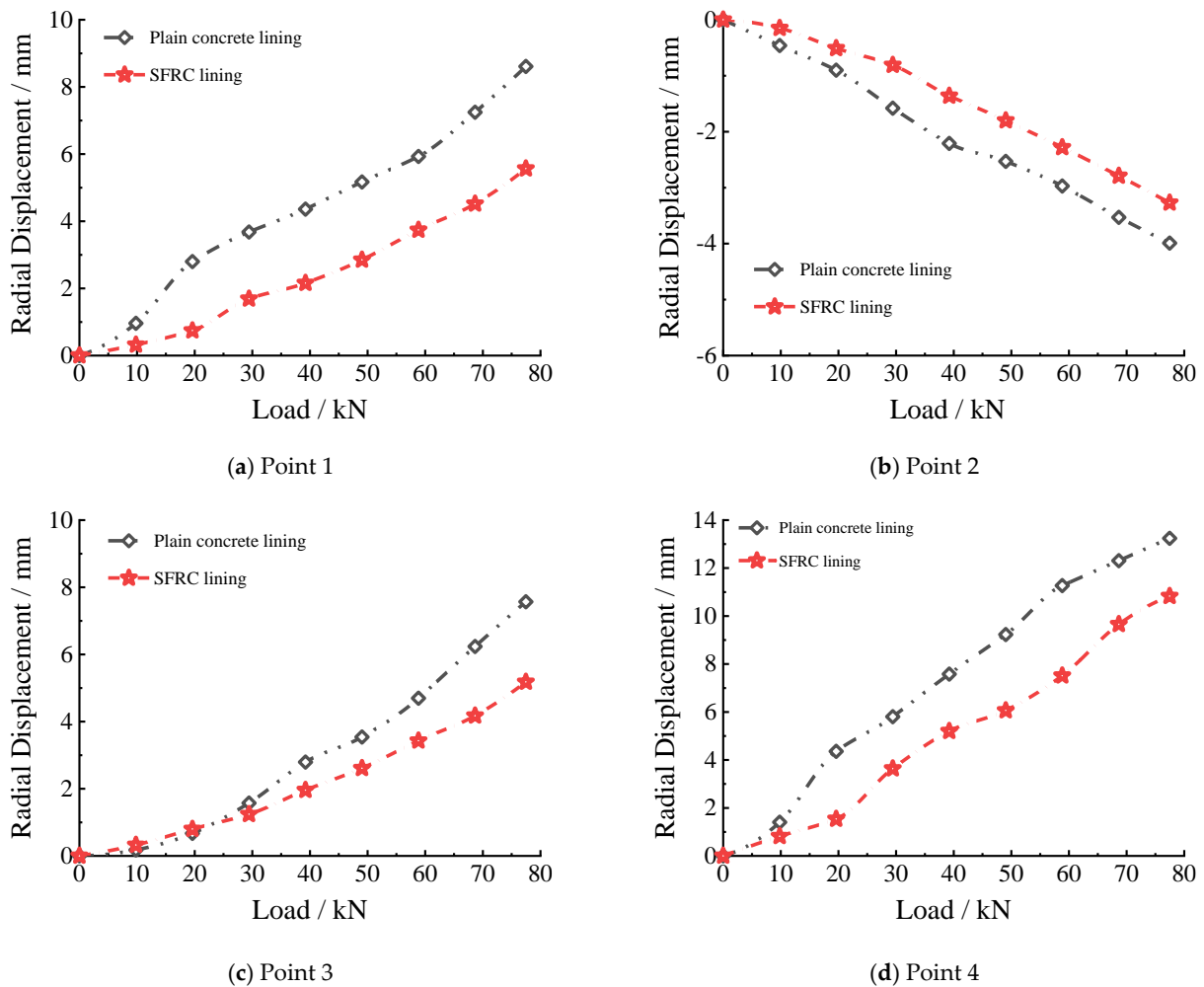


Figure 17. Load–displacement curves of single-layer lining models.

3.2.4. Internal Force and the Safety of the Lining

After the completion of the loading test, the axial force and bending moment of the lining structures was calculated according to Equations (1) and (2) based on the measured strain sum of the inner (ε_i) and outer (ε_o) sides of the lining structure.

$$N = \frac{1}{2}E(\varepsilon_i + \varepsilon_o)bh \quad (1)$$

$$M = \frac{1}{12}E(\varepsilon_i - \varepsilon_o)bh^2 \quad (2)$$

In Equations (1) and (2), h , E and b are the thickness, elastic modulus, and unit length of the lining (1 m), respectively. The distributions of calculated axial force and bending moments along the lining section are shown in Figure 18.

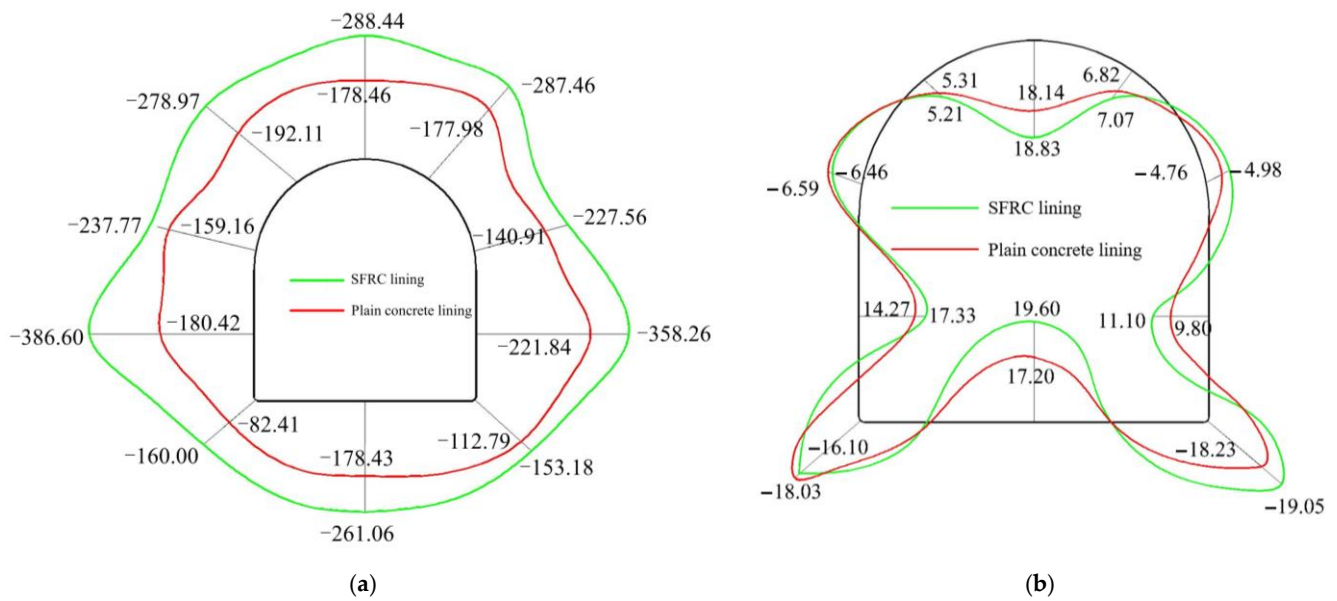


Figure 18. Internal force distributions of single-layer linings. (a) Axial force distribution of single-layer linings, (b) Bending moment distribution of single-layer linings.

It can be seen from Figure 18a that the axial force of the SFRC single-layer lining is greater than that of the plain concrete single-layer lining. At the arch crown, the axial force value of the SFRC single-layer lining is -288.44 kN, and the axial force value of the plain concrete single-layer lining is -178.46 kN, which is 0.62 times that of the SFRC single-layer lining. At the bottom plate of the lining, the axial force of the SFRC single-layer lining is 1.46 times that of the plain concrete single-layer lining, and the minimum axial force of the two lining structures appears at the foot of the wall. Additionally, the axial force distribution map has a certain symmetry, representing a roughly ‘maple leaf’ type. The bending moment at the arch crown of the SFRC single-layer lining is 18.83 kN·m, and the bending moment at the arch crown of the plain concrete single-layer lining is 18.14 kN·m. The flexural performance of the SFRC single-layer lining is 3.8% higher than that of the plain concrete single-layer lining, as shown in Figure 18b. In the middle of the bottom plate of the lining, the bending moment of the SFRC single-layer lining is 19.60 kN·m, which is 1.14 times that of the single-layer lining made of plain concrete. The bending moments of the two lining structures at the foot of the wall, the arch crown, and the bottom plate are large, indicating that the bending capacity of the lining section should be strictly controlled in terms of the lining’s design and construction.

According to the axial force and bending moment values of the lining calculated in the above section, and the Guidelines for the Design of Highway Tunnels (JTG/T D70-2010) [51], when $e_0 \leq 0.2h$, this represents the compressive strength control bearing capacity, otherwise it represents the tensile strength control bearing capacity. The formula for calculating the safety factor of compressive strength is shown in Equation (3), and Equation (4) can be used for calculating the safety factor of tensile strength. The distribution of safety factors along the lining section is shown in Figure 19.

$$KN \leq \varphi\alpha R_a bh \quad (3)$$

$$KN \leq \frac{1.75R_l bh}{\frac{6e_0}{h} - 1} \quad (4)$$

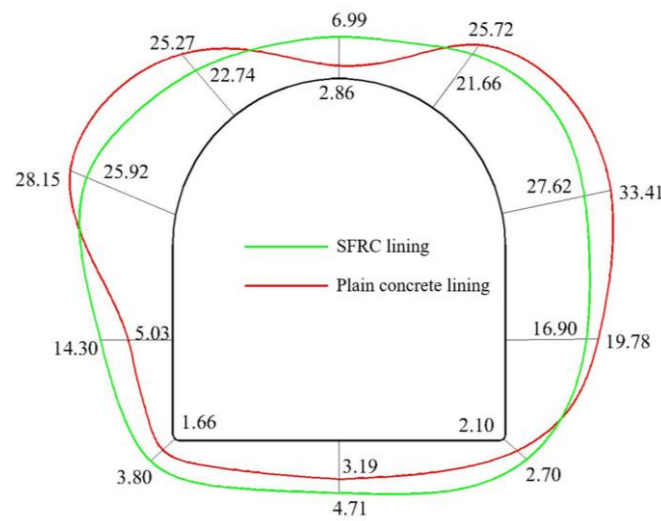


Figure 19. Safety factor distribution of the main parts of the single-layer linings.

K is the safety factor; N is the axial force (kN); φ is the longitudinal bending coefficient of the component; α is the eccentric influence coefficient of axial force; and R_a and R_t are the compressive and tensile ultimate strength (MPa) of concrete, respectively. b is the width of the cross section (1 m); h is the section's thickness (m); and e_0 is the eccentricity.

It is found that the safety factors of the two lining structures are small at the foot of the wall, the bottom plate, and the arch crown, as well as the side wall. According to the Guidelines for the Design of Highway Tunnels (JTG/T D70-2010) [51], when concrete reaches the limit of tensile strength, the safety factor shall not be less than 2.7. The safety factors of the single-layer plain concrete lining at the left and right wall corner are 1.66 and 2.10 (both under tension control), with both safety factors less than 2.7; thus, the left and right wall corner cannot meet safety requirements. Conversely, the safety factors of each part of the SFRC single-layer lining are greater than the safety factor regulatory limit specified in the Guidelines for the Design of Highway Tunnels (JTG/T D70-2010) [51]. The safety factor is the minimum value of 2.7 at the right wall corner, followed by 3.8 at the left wall corner, which is 1.3 times and 2.3 times the safety factor of the corresponding position of the plain concrete single-layer lining (the safety factor is increased by 28.6% and 128.9%, respectively). At the arch crown, although the safety factor of the plain concrete single-layer lining meets the requirements of the specification, it is close to the critical value of the safety factor and the safety reserve is relatively weak; the SFRC single-layer lining has a large safety reserve at the vault, and the safety factor is 6.99, which is 2.4 times that of the plain concrete single-layer lining.

4. Discussion

This study determined the recommended content of steel fibers in concrete used in tunnel linings to be 45 kg/m^3 and the recommended aspect ratio to be 70 through laboratory experiments. Based on these recommended parameters, similar model tests were conducted to investigate the cracking patterns and load-bearing performance of SFRC tunnel linings compared to plain concrete tunnel linings.

During the model tests, it was observed that the initial cracking load of the plain concrete single-layer lining was 0.027 MPa, while the SFRC single-layer lining had an initial cracking load of 0.04 MPa. This represents a significant increase of 48.1% in the initial cracking load compared to the plain concrete lining. Additionally, the SFRC single-layer lining exhibited a higher number of meandering and intricate cracks compared to the plain concrete lining. The presence of steel fibers in SFRC contributes to its high strength and anchoring effect within the concrete matrix, resulting in excellent ductility and toughness. This effectively enhances the overall tensile strength of SFRC, resists crack propagation, and, to some extent, limits the length and width of cracks. In contrast, the plain concrete

lining lacks the reinforcing effect of steel fibers, making crack formation easier and resulting in wider cracks. Moreover, steel fibers in concrete disperse and bear partial loads, leading to multiple instances of local cracking. However, this does not lead to overall failure of the lining structure, thus demonstrating the stronger load-bearing capacity of SFRC.

Furthermore, the SFRC exhibited smaller radial displacements than the plain concrete lining. This can be attributed to the effective control and mitigation of crack expansion provided by the presence of steel fibers. Steel fibers also improved the stiffness and deformation resistance of the lining, further reducing radial displacements under load. On the other hand, the plain concrete lining, lacking steel fiber reinforcement, demonstrated weaker toughness, lower crack resistance, and easier crack expansion. Additionally, its relatively lower stiffness led to larger radial displacements.

In summary, the inclusion of steel fibers in concrete provides significant advantages to SFRC linings. It enhances their strength, stiffness, load-bearing capacity, and crack resistance. SFRC linings exhibit improved durability, thereby contributing to the extension of tunnel service life by offering enhanced technical parameters.

5. Conclusions

This paper investigated the influence of steel fiber content and aspect ratio on the mechanical properties of concrete. Based on the limited experimental program and the reference literature on SFRC, the recommended steel fiber content and aspect ratio were determined. Furthermore, the paper proposes a mix ratio for similar tunnel-surrounding rock and lining materials. It also analyzes the cracking pattern and safety of SFRC single-layer linings. The main conclusions of this paper are as follows:

- (1) Steel fiber has a limited effect on the compressive strength and elastic modulus of concrete. It is recommended that the steel fiber content of concrete used in single-layer linings is 45 kg/m^3 . When the steel fiber content is 45 kg/m^3 , equivalent to a volume fraction of 0.58%, the cubic compressive strength of concrete reaches 44.9 MPa, axial compressive strength reaches 33.7 MPa, and the elastic modulus reaches 37.2 GPa. Steel fibers with an aspect ratio of 70 have a better effect on the axial compressive strength and elastic modulus of concrete compared to steel fibers with an aspect ratio of 50.
- (2) The initial cracking load of the SFRC lining model was 0.04 MPa, which is 48.1% higher than the initial cracking load of the plain concrete lining model (0.027 MPa). This demonstrates that SFRC is capable of significantly enhancing the initial cracking load of lining structures.
- (3) When loaded to 78.45 kN, the axial force in the SFRC single-layer lining at the arch crown of the lining was 1.62 times higher than that in the plain concrete single-layer lining. Similarly, the axial force in the SFRC single-layer lining at the bottom of the lining was 1.46 times greater than that in the plain concrete single-layer lining. Moreover, the axial force distribution map exhibits a symmetrical pattern resembling a 'maple leaf'.
- (4) When loaded to 78.45 kN, both types of lining structures exhibited significant bending moments at the foot of the wall, arch crown, and bottom plate. This indicates the necessity of carefully controlling the bending capacity of the lining section during design and construction. The minimum safety factor at the corner of the plain concrete single-layer lining was 1.66, while the minimum safety factor at the corner of the SFRC single-layer lining was 2.70. This indicates that the inclusion of steel fibers improved the safety of the lining structure by 62.7%.

Author Contributions: Conceptualization, H.L. and Y.W.; formal analysis, Y.W. and A.Z.; funding acquisition, H.L. and F.L.; investigation, Z.L. and K.Z.; methodology, H.L. and Z.L.; project administration H.L. and Z.L.; supervision H.L., Y.W. and B.Z.; validation, H.L. and A.Z.; writing—original draft, H.L., Y.W. and Z.L.; writing—review and editing B.Z., F.L. and K.Z. All authors have read and agreed to the published version of the manuscript.

Funding: This work was supported by the National Natural Science Foundation of China (Grant No. 51608450) and the Natural Science Foundation of Sichuan Province (No. 2022NSFSC1025).

Institutional Review Board Statement: Not applicable.

Informed Consent Statement: Not applicable.

Data Availability Statement: The data presented in this study are available on request from the corresponding author.

Conflicts of Interest: The authors declare there are no conflict of interest.

References

1. Ministry of Housing and Urban Rural Development of the People's Republic of China. *Technical Specification for Application of Fiber Reinforced Concrete*; China Architecture & Building Press: Beijing, China, 2010.
2. Qin, S.; Gao, D.; Wang, Z.; Zhu, H. Research on the Fracture Behavior of Steel-Fiber-Reinforced High-Strength Concrete. *Materials* **2021**, *15*, 135. [[CrossRef](#)] [[PubMed](#)]
3. Plizzari, G.A.; Tiberti, G. Steel Fibers as Reinforcement for Precast Tunnel Segments. *Tunn. Undergr. Space Technol.* **2006**, *21*, 438–439. [[CrossRef](#)]
4. Cui, G.; Wang, X.; Wang, D. Study on the Model Test of the Antibreaking Effect of Fiber Reinforced Concrete Lining in Tunnel. *Shock Vib.* **2020**, *2020*, 5419650. [[CrossRef](#)]
5. Xu, G.; He, C.; Yang, Q.; Wang, B. Progressive Failure Process of Secondary Lining of a Tunnel under Creep Effect of Surrounding Rock. *Tunn. Undergr. Space Technol.* **2019**, *90*, 76–98. [[CrossRef](#)]
6. Rossi, P.; Coussy, O.; Boulay, C.; Acker, P.; Malier, Y. Comparison between Plain Concrete Toughness and Steel Fibre Reinforced Concrete Toughness. *Cem. Concr. Res.* **1986**, *16*, 303–313. [[CrossRef](#)]
7. Liu, X.; Sun, Q.; Song, W.; Bao, Y. Structural Behavior of Reinforced Concrete Tunnel Linings with Synthetic Fibers Addition. *Tunn. Undergr. Space Technol.* **2023**, *131*, 104771. [[CrossRef](#)]
8. Wang, X.; Fan, F.; Lai, J.; Xie, Y. Steel Fiber Reinforced Concrete: A Review of Its Material Properties and Usage in Tunnel Lining. *Structures* **2021**, *34*, 1080–1098. [[CrossRef](#)]
9. Tadepalli, P.R.; Mo, Y.L.; Hsu, T.T.C. Mechanical Properties of Steel Fibre Concrete. *Mag. Concr. Res.* **2013**, *65*, 462–474. [[CrossRef](#)]
10. Khabaz, A. Performance Evaluation of Corrugated Steel Fiber in Cementitious Matrix. *Constr. Build. Mater.* **2016**, *128*, 373–383. [[CrossRef](#)]
11. Li, Z.; Wu, M.; Wu, J.; Cui, Y.; Xue, X. Steel Fibre Reinforced Concrete Meso-Scale Numerical Analysis. *Adv. Civ. Eng.* **2020**, *2020*, 2084646. [[CrossRef](#)]
12. Zhang, P.; Li, Q.; Wang, J.; Shi, Y.; Ling, Y. Effect of PVA Fiber on Durability of Cementitious Composite Containing Nano-SiO₂. *Nanotechnol. Rev.* **2019**, *8*, 116–127. [[CrossRef](#)]
13. Abbass, W.; Khan, M.I.; Mourad, S. Evaluation of Mechanical Properties of Steel Fiber Reinforced Concrete with Different Strengths of Concrete. *Constr. Build. Mater.* **2018**, *168*, 556–569. [[CrossRef](#)]
14. Khabaz, A. Monitoring of Impact of Hooked Ends on Mechanical Behavior of Steel Fiber in Concrete. *Constr. Build. Mater.* **2016**, *113*, 857–863. [[CrossRef](#)]
15. Zhang, L.; Zhao, J.; Fan, C.; Wang, Z. Effect of Surface Shape and Content of Steel Fiber on Mechanical Properties of Concrete. *Adv. Civ. Eng.* **2020**, *2020*, 8834507. [[CrossRef](#)]
16. Al-Masoodi, A.H.H.; Kawan, A.; Kasmuri, M.; Hamid, R.; Khan, M.N.N. Static and Dynamic Properties of Concrete with Different Types and Shapes of Fibrous Reinforcement. *Constr. Build. Mater.* **2016**, *104*, 247–262. [[CrossRef](#)]
17. Radojičić, V.; Radulović, R.; Tarić, M.; Jović, S. The Influence of the Steel Fibers on Improvement of Mechanical Characteristic of Concrete. *Mech. Based Des. Struct. Mach.* **2022**, *50*, 2929–2939. [[CrossRef](#)]
18. Liao, L.; Zhao, J.; Zhang, F.; Li, S.; Wang, Z. Experimental Study on Compressive Properties of SFRC under High Strain Rate with Different Fiber Content and Aspect Ratio. *Constr. Build. Mater.* **2020**, *261*, 119906. [[CrossRef](#)]
19. Niu, D.; Jiang, L.; Bai, M.; Miao, Y. Study of the Performance of Steel Fiber Reinforced Concrete to Water and Salt Freezing Condition. *Mater. Des.* **2013**, *44*, 267–273. [[CrossRef](#)]
20. Xu, H.; Shao, Z.; Wang, Z.; Cai, L.; Li, Z.; Jin, H.; Chen, T. Experimental Study on Mechanical Properties of Fiber Reinforced Concrete: Effect of Cellulose Fiber, Polyvinyl Alcohol Fiber and Polyolefin Fiber. *Constr. Build. Mater.* **2020**, *261*, 120610. [[CrossRef](#)]
21. Han, J.; Zhao, M.; Chen, J.; Lan, X. Effects of Steel Fiber Length and Coarse Aggregate Maximum Size on Mechanical Properties of Steel Fiber Reinforced Concrete. *Constr. Build. Mater.* **2019**, *209*, 577–591. [[CrossRef](#)]
22. Han, J.; Huang, D.; Chen, J.; Lan, X. Experiment Study and Finite Element Analysis of the Coupling Effect of Steel Fiber Length and Coarse Aggregate Maximum Size on the Fracture Properties of Concrete. *Crystals* **2021**, *11*, 850. [[CrossRef](#)]
23. Ige, O.; Barnett, S.; Chiverton, J.; Nassif, A.; Williams, J. Effects of Steel Fibre-Aggregate Interaction on Mechanical Behaviour of Steel Fibre Reinforced Concrete. *Adv. Appl. Ceram.* **2017**, *116*, 193–198. [[CrossRef](#)]
24. de la Fuente, A.; Pujadas, P.; Blanco, A.; Aguado, A. Experiences in Barcelona with the Use of Fibres in Segmental Linings. *Tunn. Undergr. Space Technol.* **2012**, *27*, 60–71. [[CrossRef](#)]

25. Caratelli, A.; Meda, A.; Rinaldi, Z.; Romualdi, P. Structural Behaviour of Precast Tunnel Segments in Fiber Reinforced Concrete. *Tunn. Undergr. Space Technol.* **2011**, *26*, 284–291. [[CrossRef](#)]
26. Johnson, R.P.; Psomas, S.; Eddie, C.M. Design of Steel Fibre Reinforced Concrete Tunnel Linings. *Proc. Inst. Civ. Eng.-Struct. Build.* **2017**, *170*, 115–130. [[CrossRef](#)]
27. Caratelli, A.; Meda, A.; Rinaldi, Z. Design According to MC2010 of a Fibre-Reinforced Concrete Tunnel in Monte Lirio, Panama. *Struct. Concr.* **2012**, *13*, 166–173. [[CrossRef](#)]
28. Ding, Y.; Liu, H.; Pacheco-Torgal, F.; Jalali, S. Experimental Investigation on the Mechanical Behaviour of the Fiber Reinforced High-Performance Concrete Tunnel Segment. *Compos. Struct.* **2011**, *93*, 1284–1289. [[CrossRef](#)]
29. Buratti, N.; Ferracuti, B.; Savoia, M. Concrete Crack Reduction in Tunnel Linings by Steel Fibre-Reinforced Concretes. *Constr. Build. Mater.* **2013**, *44*, 249–259. [[CrossRef](#)]
30. Moradi, M.; Bagherieh, A.R.; Esfahani, M.R. Constitutive Modeling of Steel Fiber-Reinforced Concrete. *Int. J. Damage Mech.* **2020**, *29*, 388–412. [[CrossRef](#)]
31. Kong, C.; Wang, H.; Zhao, K.; Gao, X. Numerical Simulation of Long-Term Deterioration of Rock Mass Supported by Shotcrete Lining. *Front. Earth Sci.* **2022**, *10*, 891084. [[CrossRef](#)]
32. Xu, G.; He, C.; Wang, J.; Zhang, J. Study on the Damage Evolution of Secondary Tunnel Lining in Layered Rock Stratum. *Bull. Eng. Geol. Environ.* **2020**, *79*, 3533–3557. [[CrossRef](#)]
33. Wang, S.; Wang, Y.; Lin, Z.; Song, Z.; Wang, X.; Peng, X. Analysis of the Influence of the Thickness Insufficiency in Secondary Lining on the Mechanical Properties of Double-Layer Lining of Shield Tunnel. *Eng. Fail. Anal.* **2022**, *141*, 106663. [[CrossRef](#)]
34. General Administration of Quality Supervision; Inspection and Quarantine of the People's Republic of China. *Fly Ash Used for Cement and Concrete*; Standards Press of China: Beijing, China, 2017.
35. China Association for Engineering Construction Standardization. *Standard Test Methods for Fiber Reinforced Concrete*; China Planning Press: Beijing, China, 2010.
36. Ministry of Housing and Urban Rural Development of the People's Republic of China. *Standard for Test Methods of Concrete Physical and Mechanical Properties*; China Architecture & Building Press: Beijing, China, 2019.
37. Ezeldin, A.S.; Balaguru, P.N. Normal- and High-Strength Fiber-Reinforced Concrete under Compression. *J. Mater. Civ. Eng.* **1992**, *4*, 415–429. [[CrossRef](#)]
38. Nataraja, M.C.; Dhang, N.; Gupta, A.P. Stress-Strain Curves for Steel-Fiber Reinforced Concrete under Compression. *Cem. Concr. Compos.* **1999**, *21*, 383–390. [[CrossRef](#)]
39. Neves, R.D.; Fernandes de Almeida, J.C.O. Compressive Behaviour of Steel Fibre Reinforced Concrete. *Struct. Concr.* **2005**, *6*, 1–8. [[CrossRef](#)]
40. Li, H.; Chen, B.; Zhu, K.; Gong, X. Flexural Toughness Test and Inversion Research on a Thermal Conductivity Formula on Steel Fiber-Reinforced Concrete Components Post-Fire. *Materials* **2022**, *15*, 5103. [[CrossRef](#)]
41. Dă, O. Experimental Research for the Effect of High Temperature on the Mechanical Properties of Steel Fiber-Reinforced Concrete. *Constr. Build. Mater.* **2015**, *75*, 82–88.
42. Zhu, Y. Study on Mechanical Characteristics of Steel Fiber Reinforced Shotcrete and Its Application in Single Layer Tunnel Lining. Ph.D. Thesis, Chongqing University, Chongqing, China, 2009.
43. Ministry of Housing and Urban Rural Development of the People's Republic of China. *Standard for Engineering Classification of Rock Mass*; China Planning Press: Beijing, China, 2015.
44. Ministry of Transport of the People's Republic of China. *Specifications for Design of Highway Tunnels Section 1 Civil Engineering*; China Communications Press: Beijing, China, 2018.
45. Wei, G.; Zhang, S.; Xiang, P. Model Test Study on the Influence of Ground Surcharges on the Deformation of Shield Tunnels. *Symmetry* **2021**, *13*, 1565. [[CrossRef](#)]
46. Liu, L.; Li, Z.; Liu, X.; Li, Y. Frost Front Research of a Cold-Region Tunnel Considering Ventilation Based on a Physical Model Test. *Tunn. Undergr. Space Technol.* **2018**, *77*, 261–279. [[CrossRef](#)]
47. Liu, K.; Guo, J.; Wan, L.; Xu, C. A Model Test Study to Optimize the Ventilation System of a Long Expressway Tunnel. *J. Wind. Eng. Ind. Aerodyn.* **2020**, *207*, 104393. [[CrossRef](#)]
48. Yu, Y.; Ling, X.; Tang, L.; Han, X.; Geng, L.; Wei, S. Preliminary Identification of the Failure Mode of Shallow Tunnels in Soil Subjected to Frost Heave: Model Test and Numerical Simulation. *Transp. Geotech.* **2021**, *29*, 100555. [[CrossRef](#)]
49. Cui, G.; Wang, D.; Ni, S.; Yuan, J.; Ma, J.; Zhu, C. Model tests on bearing characteristics of steel fiber-reinforced concrete lining of weak surrounding rock tunnel. *Chin. J. Geotech. Eng.* **2017**, *39*, 1807–1813. [[CrossRef](#)]
50. Cui, G.; Wang, L.; Wang, M.; Wang, D. Model tests for anti-breaking performance of a fiber reinforced concrete tunnel lining. *J. Vib. Shock* **2019**, *38*, 50–56+80. [[CrossRef](#)]
51. Ministry of Transport of the People's Republic of China. *Guidelines for Design of Highway Tunnel*; China Communications Press: Beijing, China, 2010.

Disclaimer/Publisher's Note: The statements, opinions and data contained in all publications are solely those of the individual author(s) and contributor(s) and not of MDPI and/or the editor(s). MDPI and/or the editor(s) disclaim responsibility for any injury to people or property resulting from any ideas, methods, instructions or products referred to in the content.